Seasonal Dependence of the Effect of Arctic Greening on Tropical Precipitation

SARAH M. KANG

School of Urban and Environmental Engineering, Ulsan National Institute of Science and Technology, Ulsan, South Korea

BAEK-MIN KIM

Division of Polar Climate Change Research, Korea Polar Research Institute, Incheon, South Korea

DARGAN M. W. FRIERSON

Department of Atmospheric Sciences, University of Washington, Seattle, Washington

SU-JONG JEONG

Jet Propulsion Laboratory, California Institute of Technology, Pasadena, California

JEONGBIN SEO AND YOOJEONG CHAE

School of Urban and Environmental Engineering, Ulsan National Institute of Science and Technology, Ulsan, South Korea

(Manuscript received 26 January 2015, in final form 19 April 2015)

ABSTRACT

This paper examines the seasonal dependence of the effect of Arctic greening on tropical precipitation. In CAM3/CLM3 coupled to a mixed layer ocean, shrub and grasslands poleward of 60°N are replaced with boreal forests. With darker Arctic vegetation, the absorption of solar energy increases, but primarily in boreal spring and summer since little insolation reaches the Arctic in boreal winter. The net energy input into the northern extratropics is partly balanced by southward atmospheric energy transport across the equator by an anomalous Hadley circulation, resulting in a northward shift of the tropical precipitation. In contrast, in boreal fall, the slight increase in insolation over the Arctic is more than offset by increased outgoing longwave radiation and reduced surface turbulent fluxes in midlatitudes, from the warmer atmosphere. As a result, the Northern Hemisphere atmosphere loses energy, which is compensated by a northward cross-equatorial atmospheric energy transport, leading to a southward shift of the tropical precipitation in boreal fall. Thus, although Arctic vegetation is changed throughout the year, its effect on tropical precipitation exhibits substantial seasonal variations.

1. Introduction

With global warming, the northern tree line is expected to advance northward; in fact, a poleward expansion of high-latitude trees has already been observed (Lloyd 2005). Since the Arctic is projected to warm dramatically compared to the rest of the world (Holland and Bitz 2003), the distribution and makeup of the Arctic biome are likely to change significantly. Indeed, model experiments with dynamic vegetation suggest that in response to doubling of CO_2, the sparsely vegetated surfaces in Arctic permafrost and tundra are replaced with extensive grasslands, and boreal forests in northern Russia and Canada expand poleward (Jeong et al. 2011). These changes in extratropical vegetation affect not only regional climate but also remote tropical climate. Arctic vegetation changes amplify high-latitude warming by reducing the albedo of the land, and by increasing atmospheric water vapor (Swann et al. 2010; Falloon et al. 2012; Chae et al. 2015). Midlatitude afforestation drives changes in the Hadley circulation, leading to a northward shift of annual mean tropical precipitation and a strengthening of the South Asian monsoon (Swann et al. 2012; McCarthy

Corresponding author address: Sarah M. Kang, School of Urban and Environmental Engineering, Ulsan National Institute of Science and Technology, UNIST-gil 50, Ulsan 689-798, South Korea. E-mail: skang@unist.ac.kr

et al. 2012). Expanded forest cover in Eurasia shifts the intertropical convergence zone (ITCZ) northward, which may explain the green Sahara in the mid-Holocene (Swann et al. 2014).

In a companion paper, Chae et al. (2015), we discuss the effect of Arctic vegetation changes on the seasonal cycle of Arctic warming. Since little insolation reaches the polar regions in winter, a reduced land surface albedo has little impact on increasing the absorbed solar energy. Hence, although Arctic vegetation is changed to a less reflecting type throughout the year, we show that Arctic warming is larger during boreal summer by a factor of 4 compared to boreal winter. Since the anomalous energy input into the Arctic caused by the vegetation change exhibits a large seasonality, its effect on the remote climate is also expected to show large seasonal variations. Shifts in tropical precipitation would affect billions of people who live in the tropics and also would change patterns of terrestrial productivity, so it is important to examine the seasonal dependence of the effect of Arctic greening on tropical precipitation.

2. Model and experiment setup

We use the NCAR Community Atmosphere Model version 3.1 (CAM3.1; Collins et al. 2004), with horizontal resolution of 2° latitude × 2.5° longitude adopting the finite-volume dynamic core and 26 hybrid-sigma levels in the vertical. CAM3.1 is coupled to a motionless slab ocean model (SOM), which allows the coupled system to generate its own sea surface temperature (SST) variability. The SOM has a spatially varying mixed layer depth. To account for ocean heat transport and model biases, a flux correction (Q flux) is applied to the SOM. The Q flux is obtained by applying the energy balance equation to the mixed layer column of the SOM, constrained with surface fluxes from the last 100 years of a 200-yr simulation with CAM3.1 run with prescribed climatological SST and sea ice conditions. Land surface processes in CAM3 are simulated with the Community Land Model version 3 (CLM3; Oleson et al. 2004) that calculates the heat, moisture, and momentum fluxes between the land surface and the atmosphere as well as thermal and hydrologic processes at the surface and in the interior of the near-surface soil layer (Bonan et al. 2002; Oleson et al. 2004; Dickinson et al. 2006). For each land surface grid cell, the vegetated portion is represented by the fractional coverage of plant functional types (PFTs).

To evaluate the effects of high-latitude vegetation changes on the climate, we run a control integration with the present-day vegetation type (denoted as CNT) and a perturbed integration with hypothetical Arctic vegetation states in the future under CO_2 doubling (denoted as VEG). The model and experiment setup are the same as in Chae et al. (2015) except for the use of the finite-volume dynamic core instead of T42 spectral dynamic core; further details of the simulations can be found in that paper. The simulations in Jeong et al. (2011) used the same atmosphere model, but coupled to the dynamic global vegetation model (DGVM; Levis et al. 2004), and showed that grasslands and shrubs in the high latitudes are replaced with boreal leaf forests in response to CO_2 doubling. Hence, in the perturbed integration (VEG), all grid points poleward of 60°N with grasslands and shrubs are converted to boreal forests, with the vegetation fixed to the current climatological condition elsewhere. We consider the extreme case of all grassland and shrubland being replaced in order to study the maximum impact of vegetation change on tropical rainfall. The imposed changes in summer leaf area index in this case are 25% larger than the simulated response to CO_2 doubling in the dynamic vegetation model study of Jeong et al. (2011). We also consider a less radical situation where only grid points with grasslands are converted to boreal forests. The results differ in magnitude, but are qualitatively very similar, so the results from the former integration with a stronger response will be shown for brevity. Each integration is conducted for 100 years and the analysis is based on the average of the last 80 years. The difference of climatological mean between VEG and CNT will be denoted as δ.

3. The hemispheric energy imbalance and tropical precipitation shift

Figure 1 shows the time mean energy budget difference due to Arctic vegetation change. The steady-state atmospheric column-integrated energy budget states that

$$R_{\mathrm{TOA}} - H = \nabla \cdot F, \tag{1}$$

where R_{TOA} is the net downward top-of-atmosphere (TOA) radiative flux, H is the net downward surface energy flux, and F is the vertically integrated moist static energy transport. Equation (1) states that the net energy input into the atmosphere is balanced by the divergence of atmospheric energy transport. When coupled to a motionless mixed layer ocean, the time mean H equals the time mean Q flux. Since the Q flux is the same between the perturbed and control integrations, there cannot be any energy transfer to the surface in the long-term mean. At monthly time scales, however, ocean heat storage can be nonzero, so that H does not equal the Q flux, and there can be significant changes in H in response to vegetation changes.
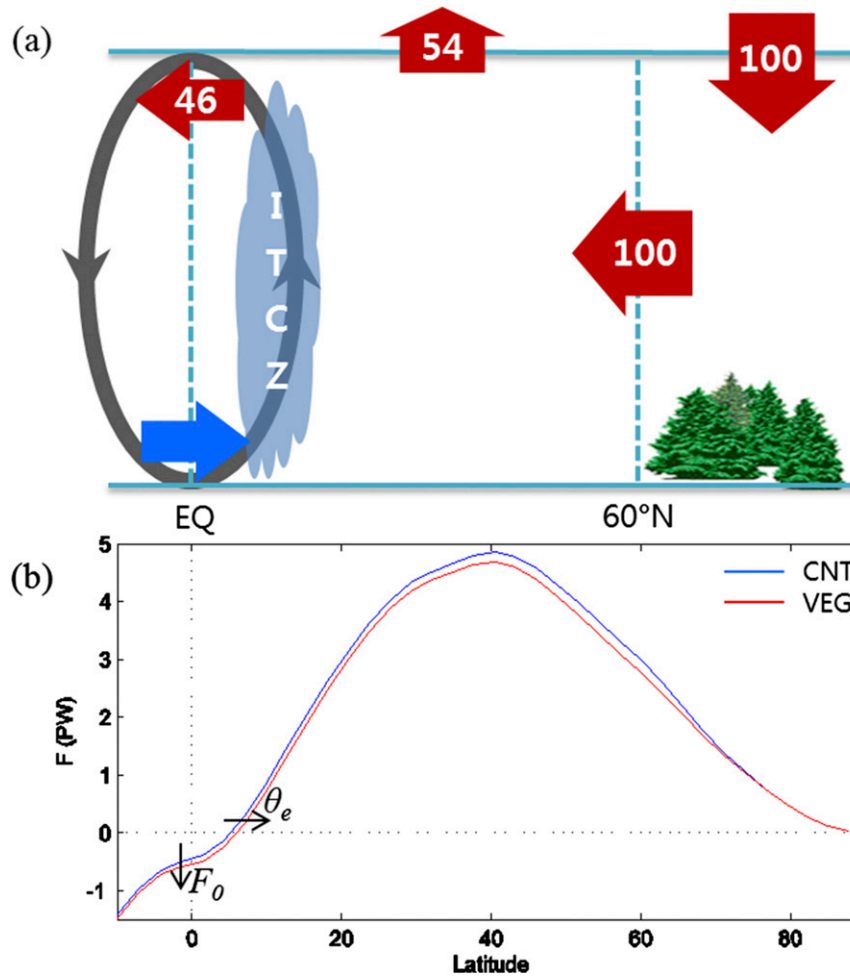
FIG. 1. (a) Schematic of the time-mean energy budget difference between VEG and CNT. With Arctic greening, there is 0.22 PW (shown as 100 units) more incoming TOA radiative flux (R_{TOA}) poleward of 60°N. Note that 46% of the surplus of R_{TOA} is transported southward across the equator. The resulting counterclockwise anomalous Hadley circulation transports moisture northward across the equator, leading to a northward shift of tropical precipitation. (b) The total atmospheric energy transport (F in PW) in CNT (blue) and VEG (red). As the southward cross-equatorial atmospheric energy transport increases (i.e., more negative F_0), the energy flux equator θ_e where F changes sign is shifted northward.

With darker Arctic vegetation, more insolation is absorbed in the northern high latitudes. As required by energy balance, in the time mean, the entire surplus of R_{TOA} is transferred to lower latitudes (i.e., southward δF at 60°N) by means of weakened eddy activity. Of the energy received by eddy fluxes in the northern extratropics, 46% is transported to the Southern Hemisphere (SH), mostly by the Hadley circulation (HC) (Fig. 1). As the northern subtropics become warmer than the southern subtropics, an anomalous HC is induced that transports energy southward across the equator, since large horizontal temperature gradients cannot be sustained in the upper tropical troposphere because of the smallness of the Coriolis parameter. The lower branch

of the anomalous HC then transports moisture northward across the equator, resulting in a northward shift of tropical precipitation.

A larger response in the HC mass transport is accompanied by larger energy and moisture transport across the equator by its upper and lower branches, respectively. Since eddy fluxes in the tropics are negligible, the energy transport by the anomalous HC explains most of the total cross-equatorial atmospheric energy transport, and the moisture transport by the anomalous HC is the main factor causing a shift of the tropical precipitation. Hence, the magnitude of the northward tropical precipitation shift is proportional to the magnitude of the southward cross-equatorial atmospheric energy transport $|\delta F_0|$. The
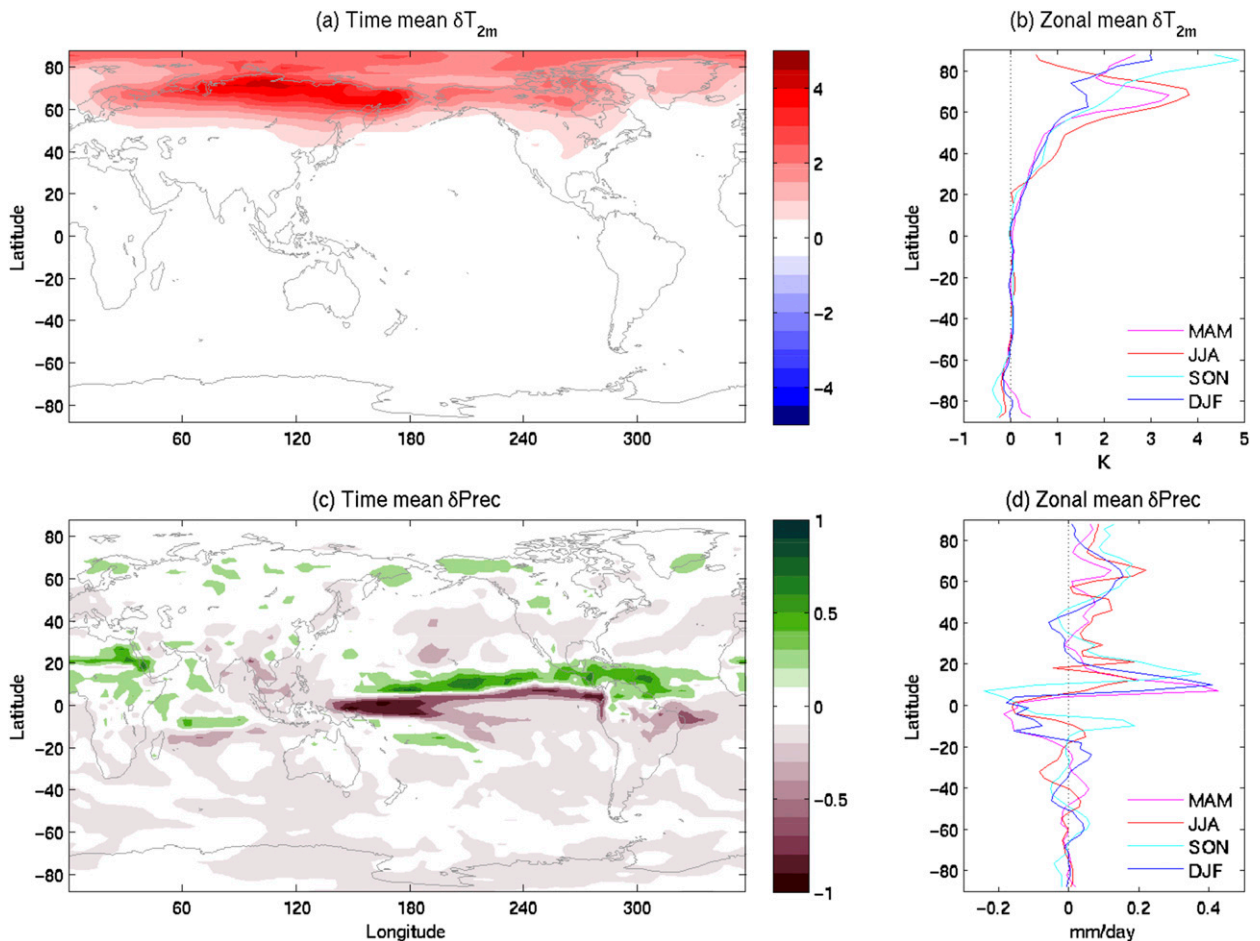
FIG. 2. The time-mean difference between VEG and CNT of the (a) lowest model level temperature (K) and (c) precipitation (mm day^{-1}).
(b),(d) The zonal means of (a) and (c), respectively, in MAM (magenta), JJA (red), SON (cyan), and DJF (blue).

anomalous southward cross-equatorial energy transport
generally leads to a northward shift of the so-called
energy flux equator θ_e where the atmospheric energy
transport changes sign, as illustrated in Fig. 1 (Kang
et al. 2008; Donohoe et al. 2013; Bischoff and Schneider
2014). The energy flux equator corresponds closely to
the ascending branch of the HC and hence the position
of the zonal-mean ITCZ. Therefore, the response of θ_e
and the magnitude of $|\delta F_0|$ will be used to infer the ex-
tent of the tropical precipitation shift.

4. Seasonal results

In response to Arctic greening, the Northern Hemi-
sphere (NH) becomes warmer, with the largest warming
of 4.7 K at 2 m in the time mean over the northern parts of
Eurasia where the vegetation type is changed (Fig. 2a).
As discussed in section 3, the differential warming in the
NH relative to the SH results in a moistening of the
northern tropics and a drying of the southern tropics in

the annual mean (Fig. 2c), consistent with Swann et al.
(2012). Since the insolation reaching the Arctic varies
greatly with the seasonal cycle, the Arctic warming is a
strong function of season (Chae et al. 2015), as is the
magnitude of the warming signal reaching the lower lat-
itudes (Fig. 2b). In particular, the northern midlatitude
warming is maximized in June–August (JJA). However,
the largest northward shift of tropical precipitation occurs
in March–May (MAM) (Fig. 2d). Following Hwang and
Frierson (2013), the response of tropical precipitation is
quantified by a tropical precipitation asymmetry index
(PAI) defined as

$$\mathrm{PAI} = \frac{P(0 - 15°\mathrm{N}) - P(15°\mathrm{S} - 0)}{P(15°\mathrm{S} - 15°\mathrm{N})},$$

where P is the zonal-mean precipitation averaged over
the latitude band indicated in parentheses. The PAI is
used to represent the tropical precipitation response
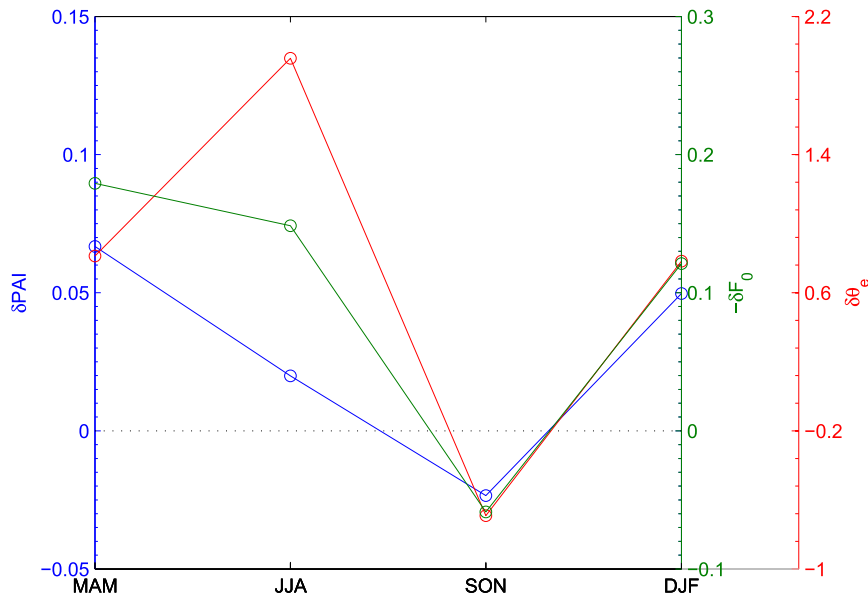since a single position such as the latitude of maximum

FIG. 3. The difference between VEG and CNT in precipitation asymmetry index δPAI (blue), negative of atmospheric energy transport between 15°S and 15°N ($-\delta F_0$) in PW (green), and energy flux equator $\delta\theta_e$ in degrees (red).

precipitation does not capture the overall pattern change. A positive change in PAI corresponds to a northward shift of tropical precipitation. The PAI response with season is shown in Fig. 3 in blue. The results presented herein are insensitive to the choice of poleward extent used for PAI. The response of precipitation centroid between 30°S/N also exhibits a similar seasonality. It is apparent from Fig. 2c that tropical precipitation shifts northward in the annual mean, as discussed in section 3 and illustrated in Fig. 1. However, the magnitude as well as the direction of the tropical precipitation response varies greatly with season. Despite yearlong changes in Arctic vegetation, the largest northward shift occurs in MAM, and, interestingly, there is a slight southward shift in September–November (SON).

For all seasons, the tropical precipitation response mostly results from changes in moisture convergence by the anomalous mass transport of the Hadley cell ($-[\overline{q_{CNT}}\nabla \cdot \delta\overline{v}]$, where q_{CNT} is the specific humidity in CNT, v is the meridional wind, and the overbar and bracket indicate the time and zonal mean and the vertical integral, respectively), as suggested by the gross similarity between the solid and dashed lines in Fig. 4. Hence, δPAI is expected to be proportional to the magnitude of anomalous atmospheric energy transport in the deep tropics, given little change in the gross moist stability (Kang et al. 2009). We note that fixed gross moist stability is not always a good assumption (Merlis et al. 2013), but it barely changes in our experiments where the extratropics are only perturbed. The absolute
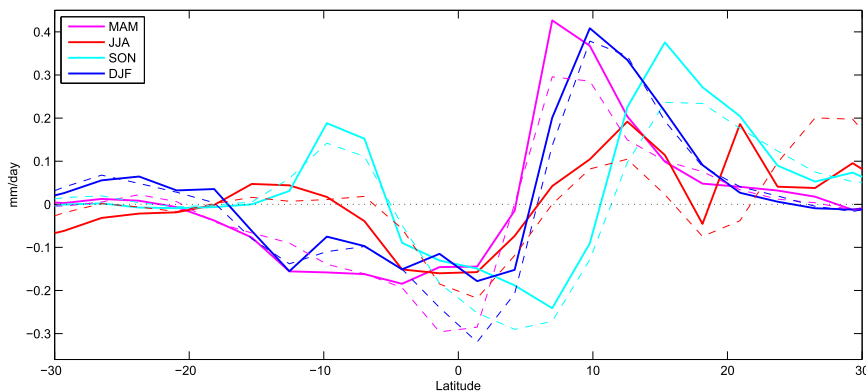

FIG. 4. The zonal-mean response of precipitation (solid) and $-[\overline{q_{CNT}}\nabla \cdot \delta\overline{v}]$ (dashed) between 30°S and 30°N in MAM, JJA, SON, and DJF in magenta, red, cyan, and blue, respectively.
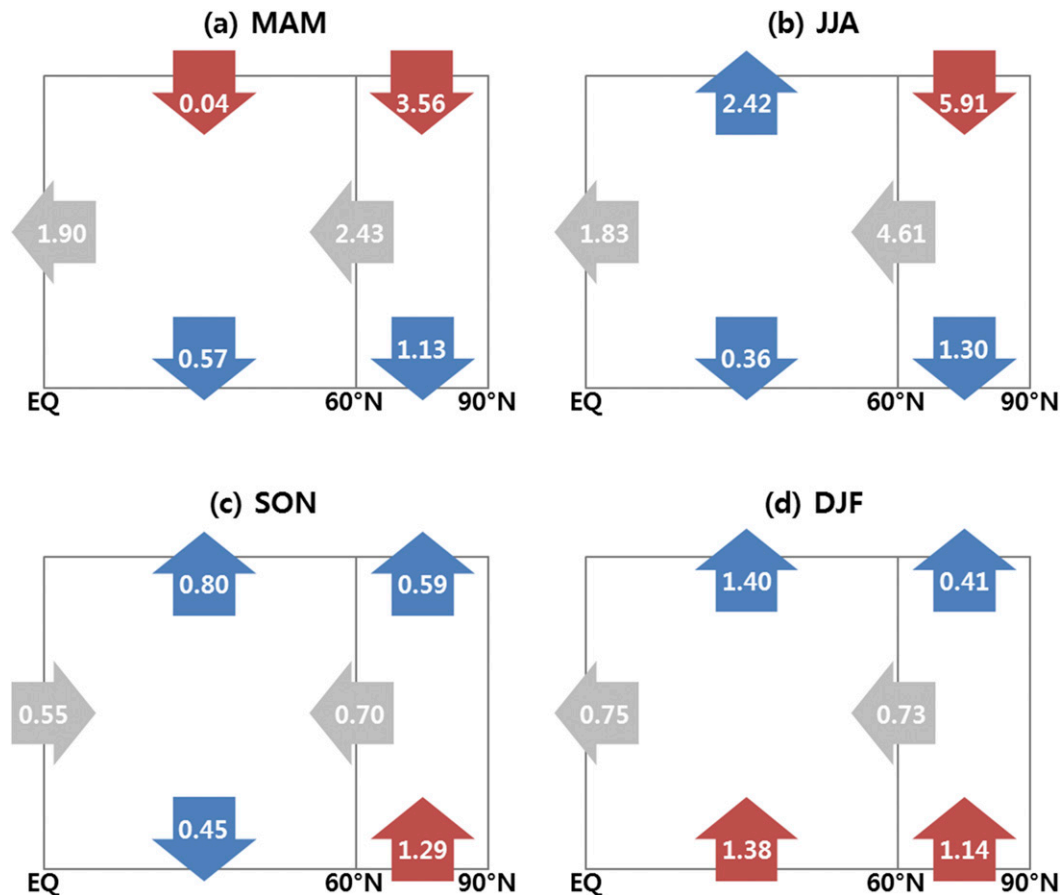
FIG. 5. Schematic of the response of the energy budget in (a) MAM, (b) JJA, (c) SON, and (d) DJF. Top and bottom arrows indicate the response of TOA radiative fluxes (δR_{TOA}) and net surface energy fluxes (H), each minus the global mean, respectively. Blue (red) corresponds to cooling (warming) the atmosphere column. Gray denotes the response of atmospheric energy transport δF at given latitude. Unit in 10^{14} W.

magnitude of the response of the atmospheric energy transport averaged over 15°S–15°N, denoted as δF_0, is plotted for each season in green in Fig. 3. Overlaid in red is the response of the energy flux equator $\delta\theta_e$, which we expect to be proportional to $|\delta F_0|$ (as discussed in section 3). Both $|\delta F_0|$ and $\delta\theta_e$ accurately predict the seasonality of tropical precipitation response, δPAI.

To understand what drives the change in F_0, we compare changes in the vertical fluxes at TOA (R_{TOA}) and surface (H), each minus the global mean, and the meridional atmospheric energy transport (F) across the equator and 60°N for each season (Fig. 5). We decompose the changes in TOA radiative fluxes (R_{TOA}) into five components, as shown in Fig. 6: shortwave radiative fluxes (SW) due to surface albedo (S_{ALB}), cloud SW (S_{CLD}) and noncloud SW (S_{NCLD}) effects, longwave clear-sky radiative fluxes (L_{CLR}), and longwave cloud radiative forcing (L_{CRF}). The TOA SW fluxes are decomposed into three terms using the approximate partial radiative perturbation (APRP) method (Taylor

et al. 2007). The surface energy flux (H) is decomposed into the shortwave, longwave, sensible heat, and latent heat fluxes (Fig. 7).

Insolation in the polar regions exhibits substantial seasonal variations, with larger amounts in MAM and JJA than SON and December–February (DJF): the net TOA shortwave flux poleward of 60°N amounts to 143 and 302 W m^{-2} versus 60 and 8 W m^{-2}, respectively. Therefore, the effect of Arctic vegetation change on a reduction in the surface albedo (S_{ALB}) is prominent only in MAM and JJA (Fig. 6, second column). Note the scale difference between MAM and JJA and between SON and DJF in Figs. 6 and 7. In MAM and JJA, the surplus of S_{ALB} in the northern Eurasia is amplified by δS_{CLD} (Fig. 6, fourth column) because of a reduction in low cloud amount (Fig. 8). Thus, the atmosphere poleward of 60°N is warmed from the TOA, but by a larger amount in JJA due to cloud feedbacks. At the surface (Fig. 7), the reduced surface albedo greatly increases the net shortwave fluxes poleward of 60°N, which is partly
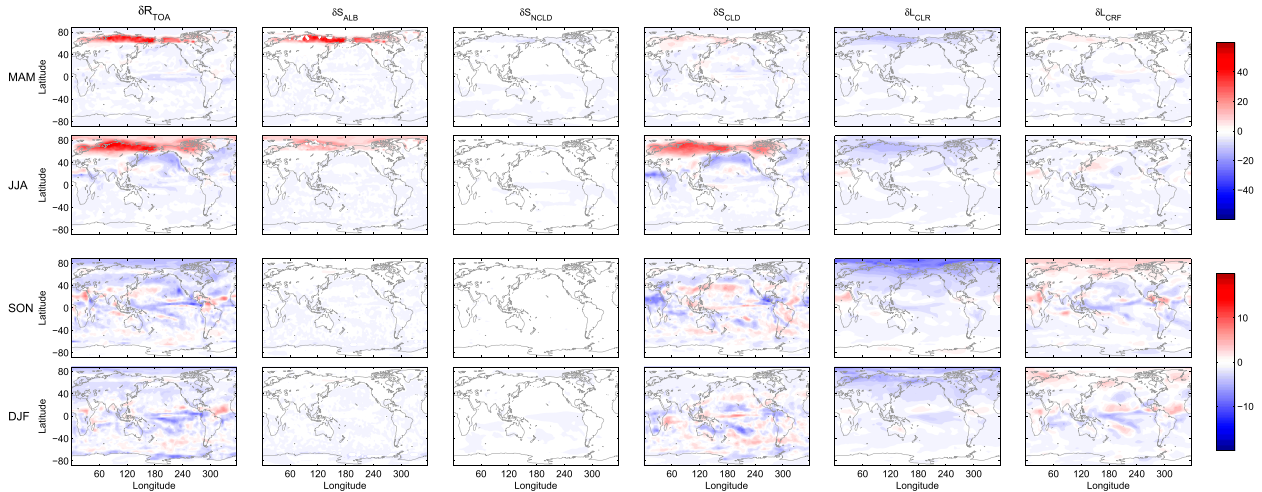
FIG. 6. The response of TOA radiative fluxes. From left to right, net flux, shortwave radiative flux decomposed into surface albedo, noncloud effects, cloud effects, longwave clear-sky radiative flux, and longwave cloud radiative forcing in (from top to bottom) MAM, JJA, SON, and DJF. Positive corresponds to downward (i.e., warming the atmosphere). Units are W m^{-2}.

compensated by an increase in upward longwave and turbulent fluxes, and partly stored in the ocean. As illustrated in Figs. 5a and 5b, the surplus of net energy input into the atmosphere poleward of 60°N is balanced by a reduction of northward atmospheric energy transport at 60°N. Between the equator and 60°N, the atmosphere is cooled at TOA in JJA due to δS_{CLD} over the northern North Pacific (Fig. 6) from increased low cloud amount (Fig. 8). The residual of about 0.19 PW is transported southward across the equator by the Hadley circulation in both MAM and JJA, which accompanies a northward shift of tropical precipitation.

In SON and DJF, little insolation reaches the polar regions, so that the effect of Arctic greening on δS_{ALB} is negligible (second column in Fig. 6), and this is more than offset by the cooling effect from δL_{CLR} from the warmer atmosphere (fifth column in Fig. 6). The cooling effect is larger in SON than in DJF because the Arctic atmosphere warms more in SON (Chae et al. 2015). This results in a large energy loss from TOA poleward of 60°N, in contrast to MAM and JJA. However, there is significant energy transfer from the surface to the overlying atmosphere via an increase in turbulent fluxes (fourth and fifth columns in Fig. 7). This surface flux is the release of energy that was stored in the ocean during MAM and JJA, and is especially concentrated over regions with sea ice loss. As a result, the atmosphere poleward of 60°N receives more energy by about 0.07 PW, which is transported southward across 60°N. Between the equator and 60°N in DJF, most of this energy flux is balanced by a southward cross-equatorial atmospheric energy transport. In SON, on the other hand, the atmosphere loses more energy at TOA (via δL_{CLR}) and

the surface than that received by transport at 60°N, resulting in a northward cross-equatorial atmospheric energy transport of 0.06 PW. The resulting anomalous Hadley circulation transports moisture southward across the equator, leading to a southward shift of tropical precipitation. Thus, the effect of a year-round change in Arctic vegetation on tropical precipitation varies widely with season due to the small insolation that reaches the Arctic during the polar night, and also due to seasonally varying climate feedbacks and energy storage. For instance, in SON, the effect of vegetation type changes on the Arctic warming is so negligible that it is overwhelmed by the midlatitude cooling that results from the warmer atmosphere emitting more L_{CLR} and reducing the surface turbulent fluxes. Hence, the NH atmosphere loses energy in SON, resulting in a northward cross-equatorial atmospheric energy transport and a southward shift of tropical precipitation, which is opposite to the time-mean response.

5. Summary and conclusions

Using the NCAR CAM3.0/CLM3.0 coupled to a mixed layer ocean, we investigate the effect of yearlong Arctic greening on the seasonality of tropical precipitation. Tropical changes in vegetation will also impact tropical precipitation, as reported in previous studies such as Seo et al. (2014) and Bischoff and Schneider (2014), but here we have focused on the effect of Arctic vegetation changes. All grid points poleward of 60°N occupied by either grasslands or shrubs are converted to boreal forests. In the time mean, the more absorbing vegetation increases the absorption of solar energy and increases surface temperature over the northern extratropics. The
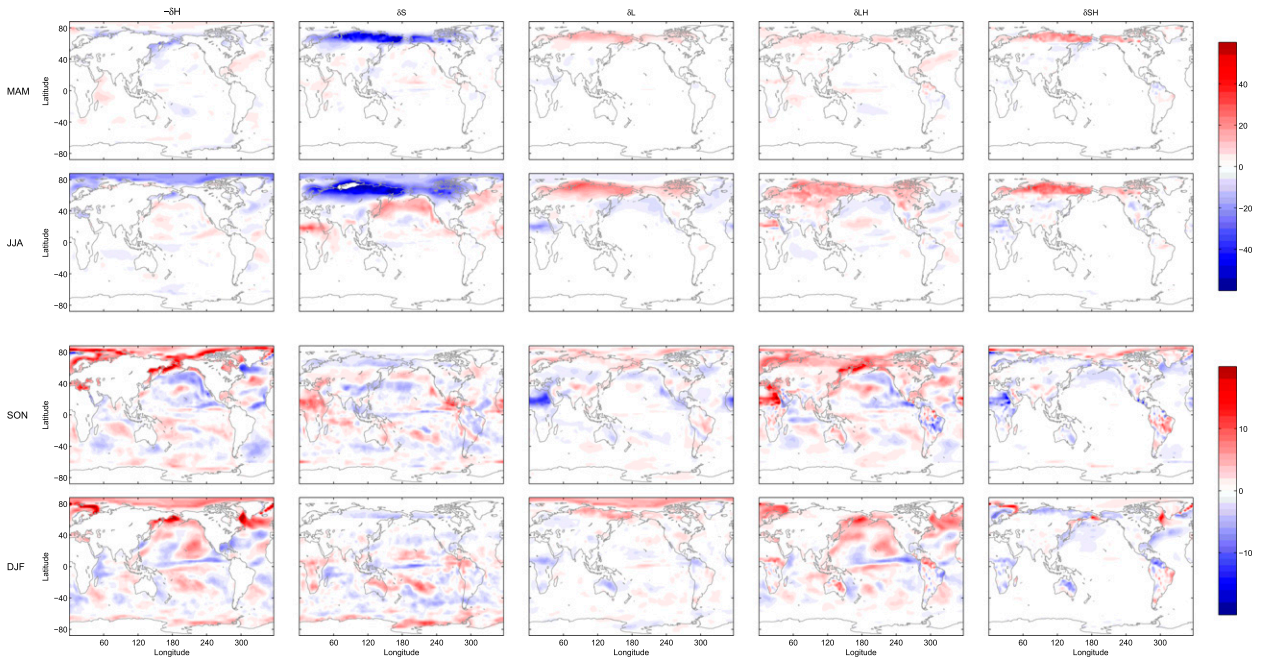
FIG. 7. The response of surface energy fluxes. From left to right, total flux, net shortwave flux, net longwave flux, latent heat flux, and sensible heat flux in (top to bottom) MAM, JJA, SON, and DJF. Positive corresponds to upward (i.e., warming the atmosphere). Units are $W\,m^{-2}$.

anomalous energy absorbed in the NH is redistributed by the Hadley circulation toward the south, resulting in a northward shift of tropical precipitation.

Arctic vegetation is changed throughout the year, so one might expect a northward shift of tropical precipitation in all seasons. However, in SON, tropical precipitation is shifted southward, in contrast to the other seasons. During polar night, little insolation reaches the Arctic so that greening induces only negligibly more absorbed solar radiation in SON and DJF. For instance, in SON and DJF, the TOA clear-sky shortwave flux poleward of 60°N is increased only by 3.24 and 1.25 $W\,m^{-2}$, as compared to 23.66 and 19.71 $W\,m^{-2}$ in MAM and JJA, respectively. In SON, the increase in shortwave is more than offset by

increased OLR from the warmer atmosphere and the surface, so that the northern extratropical atmosphere is cooled at TOA. The cooling effect at TOA is overwhelmed by increased turbulent surface fluxes from seasonal storage and diminishing sea ice cover, so that there is a slight energy input into the atmosphere at high latitudes. This anomalous energy is transported southward but is overcompensated by increased OLR and reduced turbulent surface fluxes that cool the NH atmosphere outside of the Arctic. Hence, an anomalous Hadley circulation is induced to redistribute energy northward, resulting in a southward shift of tropical precipitation.

The large seasonal variation in the tropical precipitation response to Arctic greening is due primarily to
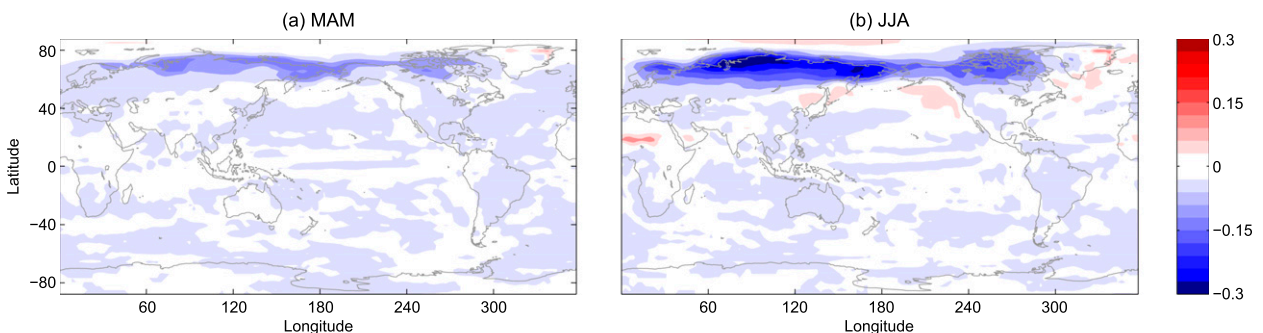

FIG. 8. The response of low cloud amount in (a) MAM and (b) JJA.

the large seasonality in insolation in the polar regions. Hence, we expect substantial seasonal dependence on the response of tropical precipitation to high-latitude climate forcing such as weakened Atlantic thermohaline circulation and Arctic sea ice loss, which have been shown to shift the annual mean ITCZ toward the warmer hemisphere (e.g., Zhang and Delworth 2005; Deser et al. 2015). In contrast, in the case where vegetation is changed outside of the polar regions, one might expect little seasonal variation in tropical precipitation response. Indeed, Swann et al. (2014) showed that expanded region of forest cover in Eurasia and grasses in the Sahara drives a northward shift of tropical precipitation consistently across seasons. In future projections, the tropical precipitation is expected to shift northward, in accordance with more warming in the NH than in the SH, although with a large amount of uncertainty (Friedman et al. 2013). Our study suggests that Arctic greening may slightly offset the northward shift of tropical precipitation in SON, while the response would be strengthened in all other seasons. However, since the results presented herein are shown to be highly dependent on cloud responses, tests with other models and convection scheme are needed to confirm the robustness of this result. The present work also suggests that we need to beware that the time-mean response does not guarantee the seasonal response.

REFERENCES

Bischoff, T., and T. Schneider, 2014: Energetic constraints on the position of the intertropical convergence zone. *J. Climate,* **27,** 4937–4951, doi:10.1175/JCLI-D-13-00650.1.

Bonan, G. B., S. Levis, L. Kergoat, and K. W. Oleson, 2002: Landscapes as patches of plant functional types: An integrating concept for climate and ecosystem models. *Global Biogeochem. Cycles,* **16** (2), doi:10.1029/2000GB001360.

Chae, Y., S. M. Kang, S.-J. Jeong, B. Kim, and D. M. W. Frierson, 2015: Arctic greening can cause earlier seasonality of polar amplification. *Geophys. Res. Lett.,* **42,** 536–541, doi:10.1002/2014GL061841.

Collins, W. D., and Coauthors, 2004: Description of the NCAR Community Atmosphere Model (CAM 3.0). NCAR Tech. Note NCAR/TN-464+STR, 214 pp.

Deser, C., R. A. Tomas, and L. Sun, 2015: The role of ocean–atmosphere coupling in the zonal mean atmospheric response to Arctic sea ice loss. *J. Climate,* **28,** 2168–2186, doi:10.1175/JCLI-D-14-00325.1.

Dickinson, R. E., K. W. Oleson, G. Bonan, F. Hoffman, P. Thornton, M. Vertenstein, Z.-L. Yang, and X. Zeng, 2006: The Community Land Model and its climate statistics as a component of the Community Climate System Model. *J. Climate,* **19,** 2302–2324, doi:10.1175/JCLI3742.1.

Donohoe, A., J. Marshall, D. Ferreira, and D. McGee, 2013: The relationship between ITCZ location and atmospheric heat transport across the equator: From the seasonal cycle to the Last Glacial Maximum. *J. Climate,* **26,** 3597–3618, doi:10.1175/JCLI-D-12-00467.1.

Falloon, P., R. Dankers, R. Betts, C. Jones, B. Booth, and F. Lambert, 2012: Role of vegetation change in future climate under the A1B scenario and a climate stabilisation scenario, using the HadCM3C Earth system model. *Biogeosciences,* **9,** 4739–4756, doi:10.5194/bg-9-4739-2012.

Friedman, A. R., Y.-T. Hwang, J. C. Chiang, and D. M. Frierson, 2013: Interhemispheric temperature asymmetry over the twentieth century and in future projections. *J. Climate,* **26,** 5419–5433, doi:10.1175/JCLI-D-12-00525.1.

Holland, M. M., and C. M. Bitz, 2003: Polar amplification of climate change in coupled models. *Climate Dyn.,* **21,** 221–232, doi:10.1007/s00382-003-0332-6.

Hwang, Y.-T., and D. M. Frierson, 2013: Link between the double–intertropical convergence zone problem and cloud biases over the Southern Ocean. *Proc. Natl. Acad. Sci. USA,* **110,** 4935–4940, doi:10.1073/pnas.1213302110.

Jeong, S.-J., C.-H. Ho, T.-W. Park, J. Kim, and S. Levis, 2011: Impact of vegetation feedback on the temperature and its diurnal range over the Northern Hemisphere during summer in a $2\times CO_2$ climate. *Climate Dyn.,* **37,** 821–833, doi:10.1007/s00382-010-0827-x.

Kang, S. M., I. M. Held, D. M. Frierson, and M. Zhao, 2008: The response of the ITCZ to extratropical thermal forcing: Idealized slab-ocean experiments with a GCM. *J. Climate,* **21,** 3521–3532, doi:10.1175/2007JCLI2146.1.

——, D. M. Frierson, and I. M. Held, 2009: The tropical response to extratropical thermal forcing in an idealized GCM: The importance of radiative feedbacks and convective parameterization. *J. Atmos. Sci.,* **66,** 2812–2827, doi:10.1175/2009JAS2924.1.

Levis, S., G. Bonan, M. Vertenstein, and K. Oleson, 2004: The Community Land Model's dynamic global vegetation model (CLM-DGVM): Technical description and user's guide. NCAR Tech. Note NCAR/TN-459+IA, 50 pp., doi:10.5065/D6P26W36.

Lloyd, A. H., 2005: Ecological histories from Alaskan tree lines provide insight into future change. *Ecology,* **86,** 1687–1695, doi:10.1890/03-0786.

McCarthy, M., J. Sanjay, B. Booth, K. Krishna Kumar, and R. Betts, 2012: Influence of vegetation on the ITCZ and South Asian monsoon in HadCM3. *Earth Syst. Dyn. Discuss.,* **3,** 91–111, doi:10.5194/esdd-3-91-2012.

Merlis, T. M., T. Schneider, S. Bordoni, and I. Eisenman, 2013: The tropical precipitation response to orbital precession. *J. Climate,* **26,** 2010–2021, doi:10.1175/JCLI-D-12-00186.1.

Oleson, K. W., and Coauthors, 2004: Technical description of the Community Land Model (CLM). NCAR Tech. Note NCAR/TN-461+STR, 173 pp., doi:10.5065/D6N877R0.

Seo, J., S. M. Kang, and D. M. W. Frierson, 2014: Sensitivity of intertropical convergence zone movement to the latitudinal position of thermal forcing. *J. Climate,* **27,** 3035–3042, doi:10.1175/JCLI-D-13-00691.1.

Swann, A. L., I. Y. Fung, S. Levis, G. B. Bonan, and S. C. Doney, 2010: Changes in Arctic vegetation amplify high-latitude warming through the greenhouse effect. *Proc. Natl. Acad. Sci. USA,* **107,** 1295–1300, doi:10.1073/pnas.0913846107.

——, ——, and J. C. Chiang, 2012: Mid-latitude afforestation shifts general circulation and tropical precipitation. *Proc. Natl. Acad. Sci. USA,* **109,** 712–716, doi:10.1073/pnas.1116706108.

——, ——, Y. Liu, and J. C. Chiang, 2014: Remote vegetation feedbacks and the mid-Holocene green Sahara. *J. Climate,* **27,** 4857–4870, doi:10.1175/JCLI-D-13-00690.1.

Taylor, K., and Coauthors, 2007: Estimating shortwave radiative forcing and response in climate models. *J. Climate,* **20,** 2530–2543, doi:10.1175/JCLI4143.1.

Zhang, R., and T. L. Delworth, 2005: Simulated tropical response to a substantial weakening of the Atlantic thermohaline circulation. *J. Climate,* **18,** 1853–1860, doi:10.1175/JCLI3460.1.